



HAL
open science

Thermoplastic elastomer obtained by photopolymerization-induced concomitant macrophase and microphase separations

Xavier Pascassio-Comte, Virginie Pellerin, Abdel Khoukh, Maud Save,
Christophe Derail, Laurent Rubatat

► To cite this version:

Xavier Pascassio-Comte, Virginie Pellerin, Abdel Khoukh, Maud Save, Christophe Derail, et al.. Thermoplastic elastomer obtained by photopolymerization-induced concomitant macrophase and microphase separations. *Journal of Polymer Science*, 2024, 62 (13), pp.2898-2909. 10.1002/pol.20240079 . hal-04595547

HAL Id: hal-04595547

<https://hal.science/hal-04595547v1>

Submitted on 28 Aug 2024

HAL is a multi-disciplinary open access archive for the deposit and dissemination of scientific research documents, whether they are published or not. The documents may come from teaching and research institutions in France or abroad, or from public or private research centers.

L'archive ouverte pluridisciplinaire **HAL**, est destinée au dépôt et à la diffusion de documents scientifiques de niveau recherche, publiés ou non, émanant des établissements d'enseignement et de recherche français ou étrangers, des laboratoires publics ou privés.

THERMOPLASTIC ELASTOMER OBTAINED BY PHOTOPOLYMERIZATION-INDUCED CONCOMITANT MACROPHASE AND MICROPHASE SEPARATIONS

*Xavier Pascassio-Comte, Virginie Pellerin, Abdel Khoukh, Maud Save, Christophe Derail, and Laurent Rubatat**

X. Pascassio-Comte, V. Pellerin, A. Khoukh, M. Save, C. Derail, L. Rubatat

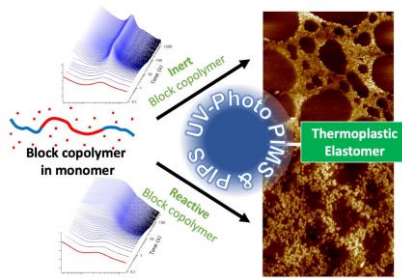
Universite de Pau et des Pays de l'Adour, E2S UPPA, CNRS, IPREM, Pau, France

E-mail: laurent.rubatat@univ-pau.fr

Abstract

We report on concomitant photoinitiated polymerization-induced macrophase and microphase separation strategies to produce hierarchically structured recyclable poly(*n*-butyl acrylate) based elastomeric materials. The investigated crosslinker-free formulations are composed of *n*-butyl acrylate monomer and a UV photo-initiator mixed with poly(methyl methacrylate)-*b*-poly(*n*-butyl acrylate)-*b*-poly(methyl methacrylate) ABA triblock copolymers. Two different pre-synthesized copolymers are used to control the macrophase separation. One synthesized by nitroxide-mediated radical polymerization (NMRP), and a second by anionic polymerization (AP). Essentially, NMRP route leads to copolymer with unsaturated chain ends, activated during photo-polymerization. On the other hand, the copolymer synthesized by AP are chemically inert during photo-polymerization. That dissimilarity is also highlighted by time-resolved FTIR and SAXS, performed to monitor respectively monomer conversion and nanostructure evolution during photo-polymerization. The experimental data demonstrate that the reactivity of the triblock copolymer impacts drastically the photopolymerization kinetics and the self-assembly processes. Finally, the rheological analysis shows that the produced materials present a solid-like behavior at low frequencies despite a large *PnBA* content (i.e., 85 wt-%). This property is associated to the phase segregation and to the sample hierarchical morphology.

Table of Content



Concomitant photopolymerization-induced macrophase and microphase separations are used to generate acrylate-based thermoplastic elastomer. The hierarchical morphologies are essentially driven by the pre-synthesized block copolymer reactivity during crosslinker-free formulations photopolymerization. The multiscale self-assembly process is monitored and highlighted by time-resolved SAXS. The resulting hierarchical materials present a solid-like behavior despite a large $PnBA$ content up to 85 wt-%.

Keywords

Photopolymerization-induced phase separation; Photopolymerization-induced microphase separation; Thermoplastic elastomer; Hierarchical structure; In situ SAXS monitoring

Introduction

Thermoplastic elastomer (TPE) is a widely commercialized class of polymer developed as coating, adhesives and more recently for 3D printing.^[1] Their elastomeric behavior under service temperatures and their thermoplastic properties at higher temperatures is compatible with classical polymer processing and recycling strategies. Among TPEs, a large part is based on block copolymers (BCPs) taking advantage of their self-assembly ability and intrinsic properties.^[1] For example, ABA triblock copolymer composed of a soft rubbery central block (majority phase) and two outer blocks with glass-transition temperature, T_g , well above service temperature.^[2] In those conditions, the glassy nanodomains act as physical crosslinks for the elastomeric matrix leading to materials displaying a solid-like behavior.^[3, 4] With that respect, polystyrene-*b*-polybutadiene-*b*-polystyrene (SBS) or polystyrene-*b*-polyisoprene-*b*-polystyrene (SIS) BCPs are commonly used as TPE. Nevertheless, the use of those copolymers presents few drawbacks, among them

the unsaturated soft blocks leading to a poor UV resistance. To overcome that issue versatile acrylic based TPEs were successfully proposed, combining low T_g polyacrylates blocks and high T_g polymethacrylates blocks, such as poly(*n*-butyl acrylate) and poly(methyl methacrylate) based BCPs.^[5-7]

BCPs self-assembly has been intensively studied during the past decades at thermodynamical equilibrium,^[8-10] including ABA triblock copolymers,^[11-15] and blends of ABA BCP with B homopolymer,^[16, 17] leading to particular rheological signatures.^[18-21] However, alternative routes are foreseen to achieve phase segregated materials such as polymerization-induced phase separation (PIPS) and polymerization-induced microphase separation (PIMS).^[22-24] Both approaches lead to kinetically arrested morphologies obtained during bulk polymerization of the monomer. PIPS macrophase separations are usually obtained when one or several pre-synthesized homopolymers are initially solubilized in monomer with crosslinker.^[25-30] On the other hand, PIMS microphase separations are reached when macro-chain transfer agents are initially solubilized in monomer with crosslinker.^[31-37] The use of pre-synthesized BCPs, initially solubilized in monomer, can also lead to PIPS and PIMS. As an example, BCPs have already been used as additives in epoxy resin formulations to bring nanostructures and to adjust the mechanical properties.^[38-43] Also, it has been reported that macrophase separations between pre-synthesized BCP and growing network can be avoided by using reactive BCPs. Thus, ensuring covalent bonds between both phases and preserving microphase segregation.^[44, 45] Among the abundant photopolymerization literature, there is a growing interest on the structural aspect of whether photoinitiated PIPS,^[26-29] or photoinitiated PIMS systems^[34, 36, 46, 47] and very recently toward stereolithography 3D printing.^[48-52]

In the present paper, we demonstrate that photoinitiated PIPS and PIMS strategies can be associated to produce hierarchically structured recyclable TPE. To do so, crosslinker-free formulations based on reactive or inert pre-synthesized ABA triblock copolymers are investigated. More specifically, formulations composed of *n*-butyl acrylate (*n*BA) monomer and UV photoinitiator in presence of a poly(methyl methacrylate)-*b*-poly(*n*-butyl acrylate)-*b*-poly(methyl methacrylate) (PMMA-*b*-P*n*BA-*b*-PMMA) triblock copolymers are prepared. Two different pre-synthesized BCPs are used: (i) one reactive, synthesized by nitroxide-mediated radical polymerization (NMRP), named T_{NMRP} , and (ii) the second inert, by anionic polymerization (AP), named T_{AP} . The comparison between both BCPs is performed through macromolecular and morphological characterizations after photopolymerization. In addition, for a better understanding of the concomitant PIPS and PIMS self-assembly processes, time-resolved FTIR and SAXS measurements are performed under UV irradiation, to monitor respectively monomer conversion and morphological evolutions. Finally, rheological properties and optical transparency of the final materials are discussed and correlated to the hierarchical morphology.

Results and Discussion

The liquid formulations are composed of pre-synthesized PMMA-*b*-PnBA-*b*-PMMA triblock, *n*BA monomer and α -hydroxy-cyclohexyl-phenyl-ketone as photoinitiator (PI) of type I. Both pre-synthesized PMMA-*b*-PnBA-*b*-PMMA triblock copolymer macromolecular characteristics are given in Table 1. All the sample formulations are listed in Table 2. The BCP weight fraction in the formulation was first optimized by solubility tests. 30 wt-% of BCP was the highest concentration achieved while preserving full solubility. Therefore, the present study focuses on that specific concentration, with two series of samples including T_{NMRP} or T_{AP} BCP and varying photoinitiator (PI) concentration. The final samples are obtained after *n*BA radical photopolymerization under a xenon-mercury UV lamp (70 mW cm⁻²) during 300 seconds (see supporting information for details).

Table 1. Characteristics of PMMA-*b*-PnBA-*b*-PMMA triblock copolymers used in this study. With M_n and M_w the number-average and weight-average molar masses respectively, D the dispersity index ($D = M_w/M_n$), and the weight fractions of the PnBA block, W_{PnBA} .

Name	Polymerization	M_n [g mol ⁻¹] ^{a)}	M_w [g mol ⁻¹] ^{a)}	D	W_{PnBA} ^{b)}
T _{NMRP}	NMRP ^{c)}	53000	81000	1.53	0.47
T _{AP}	AP ^{d)}	59000	61000	1.03	0.51

^{a)} M_n and M_w determined by SEC-MALLS using refractive index and light scattering signals, cf. Figure S1. The BCP refractive index increments (dn/dc) are given in Table S1.

^{b)} Obtained by NMR, cf. Figure S4, Figure S5 and Equation S3.

^{c)} Nitroxide mediated radical polymerization.

^{d)} Anionic polymerization.

Table 2. List of investigated formulations: weight fractions (w_x), monomer conversion (C_{nBA}) and residual monomer in the final samples (R_{nBA}).

Name	BCP	W_{BCP} [wt-%]	W_{PI} [wt-%]	W_{nBA} [wt-%]	C_{nBA} [%] ^{a)}	R_{nBA} [wt-%] ^{b)}
30T _{NMRP} PI _{0.5}	T _{NMRP}	30	0.5	69.5	96.0	2.78
30T _{NMRP} PI ₁	T _{NMRP}	30	1.0	69.0	99.8	0.14
30T _{NMRP} PI ₂	T _{NMRP}	30	2.0	68.0	99.6	0.27
30T _{NMRP} PI ₄	T _{NMRP}	30	4.0	66.0	99.8	0.13
30T _{AP} PI _{0.5}	T _{AP}	30	0.5	69.5	97.0	2.08
30T _{AP} PI ₁	T _{AP}	30	1.0	69.0	99.0	0.69
30T _{AP} PI ₂	T _{AP}	30	2.0	68.0	99.8	0.14
30T _{AP} PI ₄	T _{AP}	30	4.0	66.0	99.8	0.13

^{a)} Obtained by RT-FTIR, cf. Figure 1.

^{b)} Residual *n*BA monomer, $R_{nBA} = (100 - C_{nBA}) \times w_{nBA}$, with C_{nBA} the monomer conversion and w_{nBA} the monomer mass fraction in the formulation.

The reactivity of the T_{NMRP} neat copolymer is induced by the presence of chain end unsaturations in the outer PMMA blocks. Indeed, the poly(methyl methacrylate) propagating radicals are known to undergo β -Hydrogen transfer to the SG1 nitroxide used for T_{NMRP} copolymer synthesis, thus producing double bonds at the end of the PMMA chain.^[53, 54] The unsaturated PMMA is able to act as macromonomer in radical polymerization, as proven for unsaturated PMMA prepared by catalytic chain transfer polymerization (CCTP).^[55] To confirm this assertion ^1H NMR was performed on both BCPs. Proton NMR spectrum collected on T_{NMRP} BCP (Figure S4) reveals signals between 5 and 6.5 ppm which are assigned to unsaturated bonds.^[53] On the other hand, the T_{AP} proton NMR spectrum does not present any peak in this specific chemical shift range (Figure S5).

Figure 1 presents the *n*BA monomer conversion, measured by in situ infrared spectroscopy, for both formulated series while varying PI concentrations. As expected, polymerization kinetics get significantly faster when increasing PI concentration (Figure 1). It is worth to point out that the BCP nature also affects polymerization kinetics. Actually, $30T_{\text{AP}}$ formulations present higher polymerization rates compared to $30T_{\text{NMRP}}$ ones. Also, significant retardation and inhibition are observed exclusively on the $30T_{\text{NMRP}}$ series, those effects are reduced with PI content increase. That can be explained by the T_{NMRP} unsaturated chain ends interacting with the PI. After 300 seconds of UV exposure monomer conversions range from 96 to 99.8 % (Table 2). The lower conversion values are measured on samples with the lower PI content (0.5 wt%). Consequently, those later samples contain 2 to 3 wt-% of residual monomer (Table 2), whereas samples prepared with 4 wt-% of PI, contain a negligible amount of residual monomer.

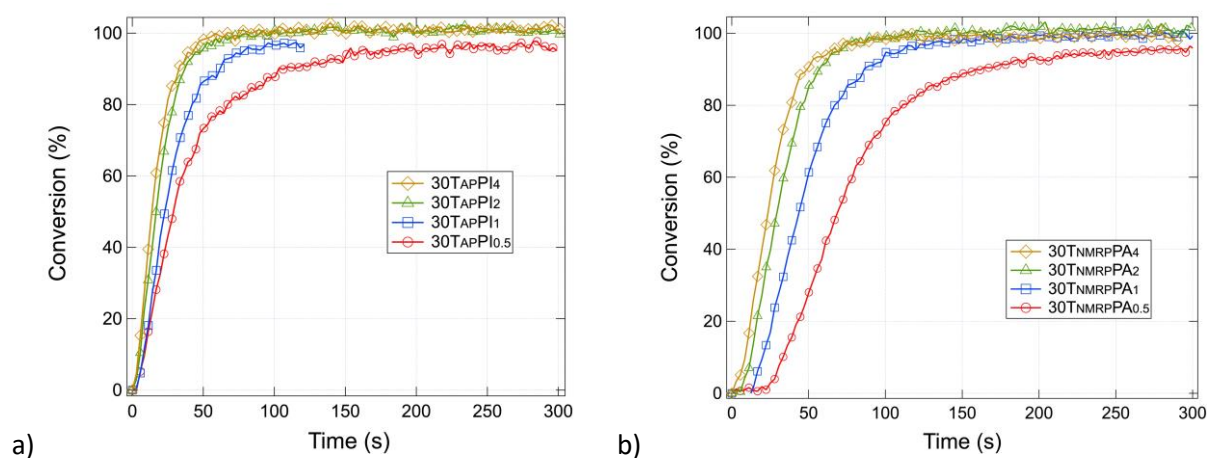
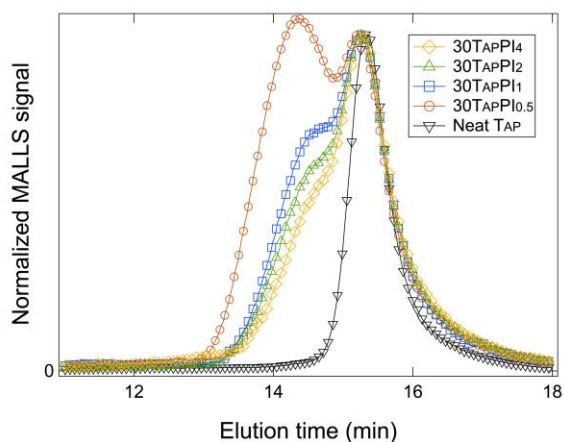
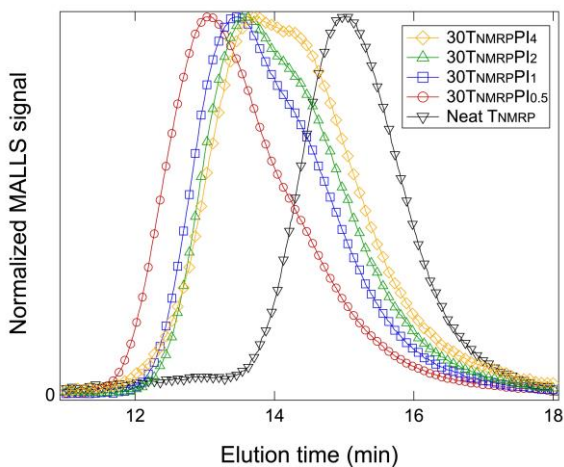


Figure 1. Monomer conversion versus time for both series at different PI concentrations: (a) T_{AP} series and (b) T_{NMRP} series. Open red circle corresponds to a PI concentration of 0.5 wt-%, open blue square to 1 wt-%, open green triangle to 2 wt-% and open orange diamond to 4 wt-%. Those conversion data are obtained by in situ RT-FTIR measurements.

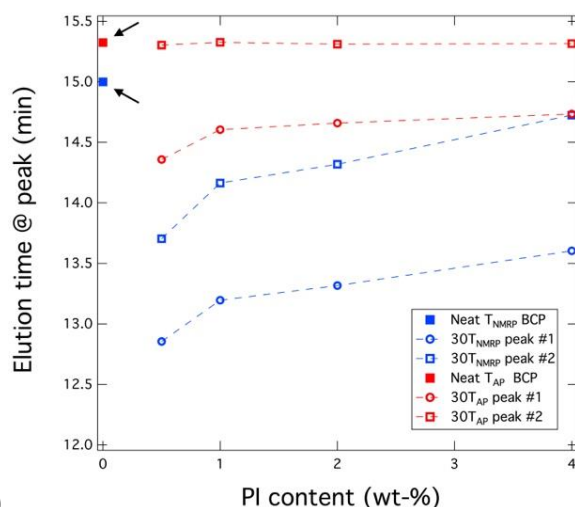
Macromolecular characterization. Both, BCPs and photopolymerized samples of both formulation series reported in Table 2 were characterized by size exclusion chromatography (SEC) as presented in Figure 2. The chromatograms of both BCPs exhibit a monomodal molar mass distribution (Figure 2), of lower dispersity and molar mass values for T_{AP} compared to T_{NMRP} (Table 1).



a)



b)



c) Figure 2. SEC MALLS signal versus elution time for both series at different PI concentrations: (a) T_{AP} series and (b) T_{NMRP} series. Open red circle corresponds to a PI concentration of 0.5 wt-%, open blue square to 1 wt-%, open green triangle to 2 wt-% and open orange diamond to 4 wt-%. (c) Elution time at maximum MALLS signal (peaks #1 and #2, determined in Figures S2 and S3) versus photoinitiator content for 30 T_{NMRP} series (blue markers) and 30 T_{AP} series (red markers). The solid markers (pointed with arrows) correspond to the neat BCPs: (blue) T_{NMRP} and (red) T_{AP} BCP.

All SEC chromatograms measured on the formulated samples present a shift of the signal toward lower elution times compared to the corresponding neat BCPs. This evidences that the weight average molar masses, of the photopolymerized resins, are larger than 61 kg mol^{-1} for 30 T_{AP} series and 81 kg mol^{-1} for the 30 T_{NMRP} one (Table 1). So, the values of M_w of the final polymer blends are then significantly higher than the entanglement molar mass of PnBA, $M_e \approx 23 \text{ kg mol}^{-1}$.^[56] The four SEC chromatograms of 30 T_{AP} formulations, whatever the PI concentration, are bimodal (Figure 2a). The peak at higher elution time (peak 2, Figure S2), is attributed to the T_{AP} BCP, since the SEC distribution matches with the neat BCP SEC trace (Figure 2). That demonstrates the non-reactivity of T_{AP} BCP. The peak, or shoulder, at lower elution time (peak 1, cf. Figure S2), which depends on PI concentration, is then attributed to the PnBA homopolymer produced in situ by photopolymerization. To accurately determine peak positions, the SEC MALLS traces are fitted with two gaussian functions, as shown on Figure S2. Then, Figure 2c present the resulting elution time at maximum intensity of MALLS signal for each different PI concentration. Elution time of peak 1 in 30 T_{AP} series slightly increases with PI concentration. That indicates the production of polymer with lower molar masses, as expected for higher initiator concentration. In parallel, DOSY NMR spectra collected on 30 $T_{\text{AP}}\text{PI}_{0.5}$ sample also confirms the inert character of the T_{AP} BCP (Figure S6c, Figure S6d and Table S2). Indeed, the diffusion coefficient associated to the PMMA peaks between 3.3 and 3.4 ppm in the formulated sample (Figure S6d) is similar to the diffusion line of the neat T_{AP} copolymer (Figure S6c). The resulting diffusion coefficients are presented in Table S2, and exhibit relatively close values for T_{AP} BCP and

30T_{AP}PI_{0.5}. This is also confirmed for other PI contents from 30T_{AP} series, all data are shown in Figure S7 and Table S2.

On the other hand, DOSY NMR spectra collected on 30T_{NMRP}PI_{0.5} sample (Figure S6b) demonstrates unambiguously a copolymer chain extension. Indeed, the diffusion coefficient associated to the PMMA peaks between 3.3 and 3.4 ppm in the formulated sample (Figure S6b) shifts toward lower diffusion coefficients compare to the neat T_{NMRP} BCP (Figure S6a), thus indicating an increase of the BCP molar mass during photo-polymerization. Similarly, this is observed for all the other PI contents, the data are presented in Figure S7 and Table S2. The corresponding SEC chromatograms of photopolymerized resins (Figure 2b) are bimodal for all PI concentrations but contrary to 30T_{AP} samples, there is a clear shift of the maxima of both SEC peaks. Both maxima of the distributions, for each bimodal chromatogram (Figure S3), are positioned at significantly lower elution time compared to the neat T_{NMRP} BCP peak, thus confirming its chain extension. Figure 2c presents the evolution of both elution time at peaks, obtained upon fitting procedure (Figure S3) as a function of PI concentration. Elution times at peak increase with PI concentration for both distributions, hence indicating a decrease of molar mass of both P_nBA homopolymer and the polymer made by T_{NMRP} chain extension during nBA photopolymerization.

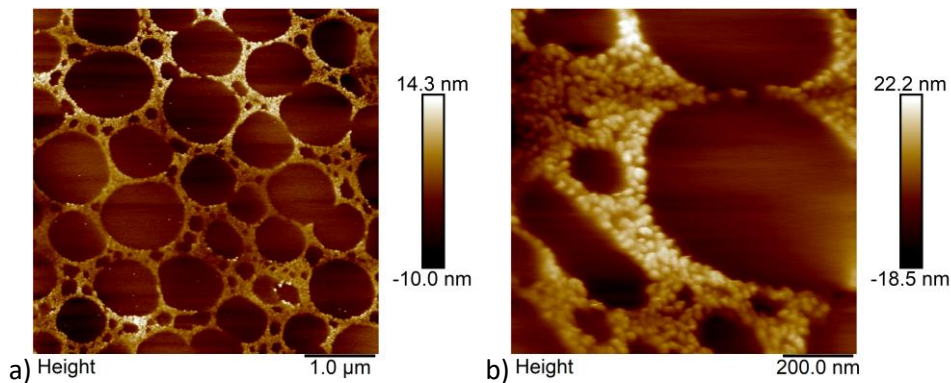


Figure 3. AFM height images collected on sample 30T_{AP}PI_{0.5} at low (a) and high (b) magnifications.

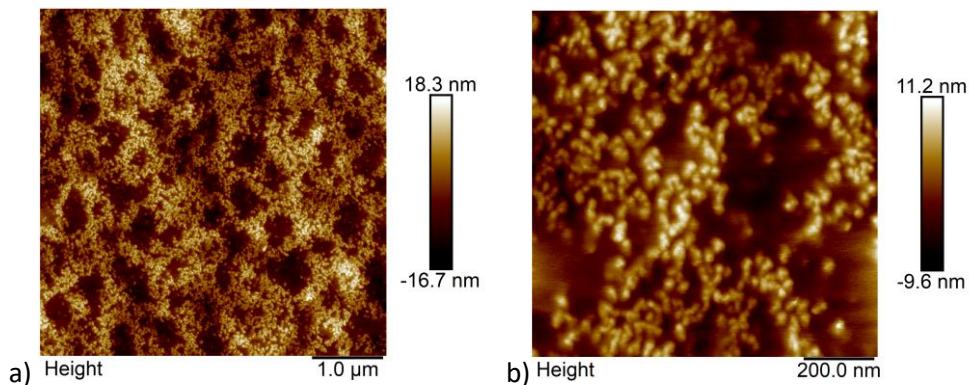


Figure 4. AFM height images collected on sample $30T_{\text{NMRP}}\text{PI}_{0.5}$ at low (a) and high (b) magnifications.

Structure characterization. The T_{AP} and T_{NMRP} neat BCP samples were solvent casted from toluene solutions, then annealed under vacuum at 120 °C during 24 hours. **Figure S8** shows the corresponding representative AFM topographic images. The morphologies are comparable for both BCPs with an evident microphase separations. The PMMA rich domains being represented by the brighter areas and the *PnBA* rich domains by the darker ones. An average characteristic distance between domains can be estimated at 25 nm for both samples (**Figure S8b and Figure S8d**). Figure 5 shows the corresponding SAXS patterns, revealing a structural peak at q^* with a weak second order peak at $2q^*$. Also, a $3q^*$ peak is slightly defined for T_{AP} BCP. That sequence of peaks may indicate a lamellar morphology, though not evidently observed by AFM. Nevertheless, SAXS confirms the AFM microphase separation with a moderate ordering and periods of 24 and 23 nm for T_{AP} and T_{NMRP} respectively.

Figure 3 and Figure 4 show topographic AFM images collected on photopolymerized formulations $30T_{\text{AP}}\text{PI}_{0.5}$ and $30T_{\text{NMRP}}\text{PI}_{0.5}$ with two different magnifications. $30T_{\text{AP}}\text{PI}_{0.5}$ sample reveals a clear macro-phase separation with a sharp interface between *PnBA* homopolymer rich macro-domains and a nano-structured percolating network of BCPs (Figure 3a and b). The macro-domains are spherical and their size distribution ranges from few tens nanometers to micrometer. At smaller length scale (Figure 3b), bright nodules of 20 ± 5 nm are associated to the BCP PMMA nano-domains within a *PnBA* matrix. On the other hand, the $30T_{\text{NMRP}}\text{PI}_{0.5}$ formulations reveals a poor macro-phase separation (Figure 4a and b). *PnBA* rich macro-phases, without well-defined contours, are surrounded by a percolating phase composed of the BCP PMMA nodules with typical dimensions of 20 ± 5 nm. It can be noticed that few PMMA nodules are also located within the *PnBA* rich macro-domains. Those hierarchical structures are repeatedly observed on $30T_{\text{AP}}$ and $30T_{\text{NMRP}}$ series respectively, with a weak dependence on PI contents (**Figures S9 and S10**). It is worth to note, that the macrophase separation variation between both series is also observable on sample transparency. $30T_{\text{NMRP}}\text{PI}_{0.5}$ sample is transparent while $30T_{\text{AP}}\text{PI}_{0.5}$ one reveals a bleaching (Figure S13). That can be attributed to a different level of macrophase separation, with a reduced fluctuation in refractive index at micrometer length scale for sample $30T_{\text{NMRP}}\text{PI}_{0.5}$.

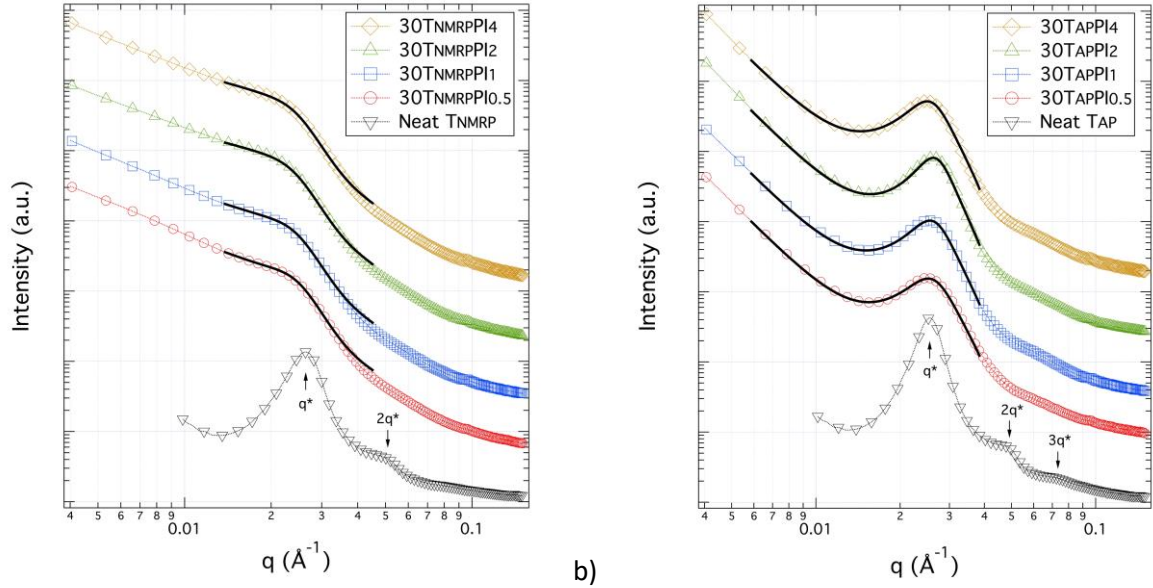


Figure 5. SAXS patterns collected on both formulations series: (a) 30T_{NMRP} series and (b) 30T_{AP} series with the respective neat BCP. Open red circle corresponds to a PI concentration of 0.5 wt-%, open blue square to 1 wt-%, open green triangle to 2 wt-% and open orange diamond to 4 wt-%. The solid black lines correspond to the Kinning–Thomas model fits.^[57] The spectra are shifted vertically for clarity. 30T_{NMRP} and 30T_{AP} series patterns were measured at synchrotron SOLEIL. Both neat BCP patterns were measured at synchrotron ALBA.

SAXS patterns are displayed on Figure 5. Spectra collected on 30T_{AP} formulations (Figure 5b) reveal a single structural peak at 0.026 \AA^{-1} , relatively close to the T_{AP} neat copolymer value. That indicates a poor insertion of the P_nBA homopolymers within BCP P_nBA blocks domains. On the other hand, 30T_{NMRP} samples do not present a well pronounced structural peak. Thus, the P_nBA might penetrate the BCP rich domains by homopolymer swelling and BCP chain extension. To extract more quantitative structural parameters, the experimental data were fitted with the Kinning-Thomas model,^[57] which is based on the Percus-Yevick hard-sphere liquid theory. This model assumes that the scattering nano-domains are spherical (cf. ESI for details). For 30T_{AP} series, an additional power law of q^{-4} is introduced in the fitting expression to account for the low- q upturn. This low- q upturn is possibly caused by the pronounced macrophase separation interfaces. The fitting results are presented in Figure 5 and Table S3. The structural parameters are in agreement with AFM observations. The spherical nano-domains are found to be about 20 nm in diameters ($2R$), weakly dependent on PI concentration and slightly higher for 30T_{NMRP} series. Also, the hard sphere radius (or closing approach radius), R_{HS} , is independent of PI content. The ratio $(R/R_{HS})^3$ (Table S3), which is the volume fraction of the PMMA phases in the hard sphere, are in agreement with BCP's compositions (Table 1). In addition, a more compact structure is observed for the 30T_{AP} series with a volume fraction of hard spheres, η , of 0.35 ± 0.03 compared to 0.24 ± 0.02 for the 30T_{NMRP} series. This corroborates the insertion of P_nBA homopolymer and T_{NMRP} BCP chain extension around the PMMA nodules.

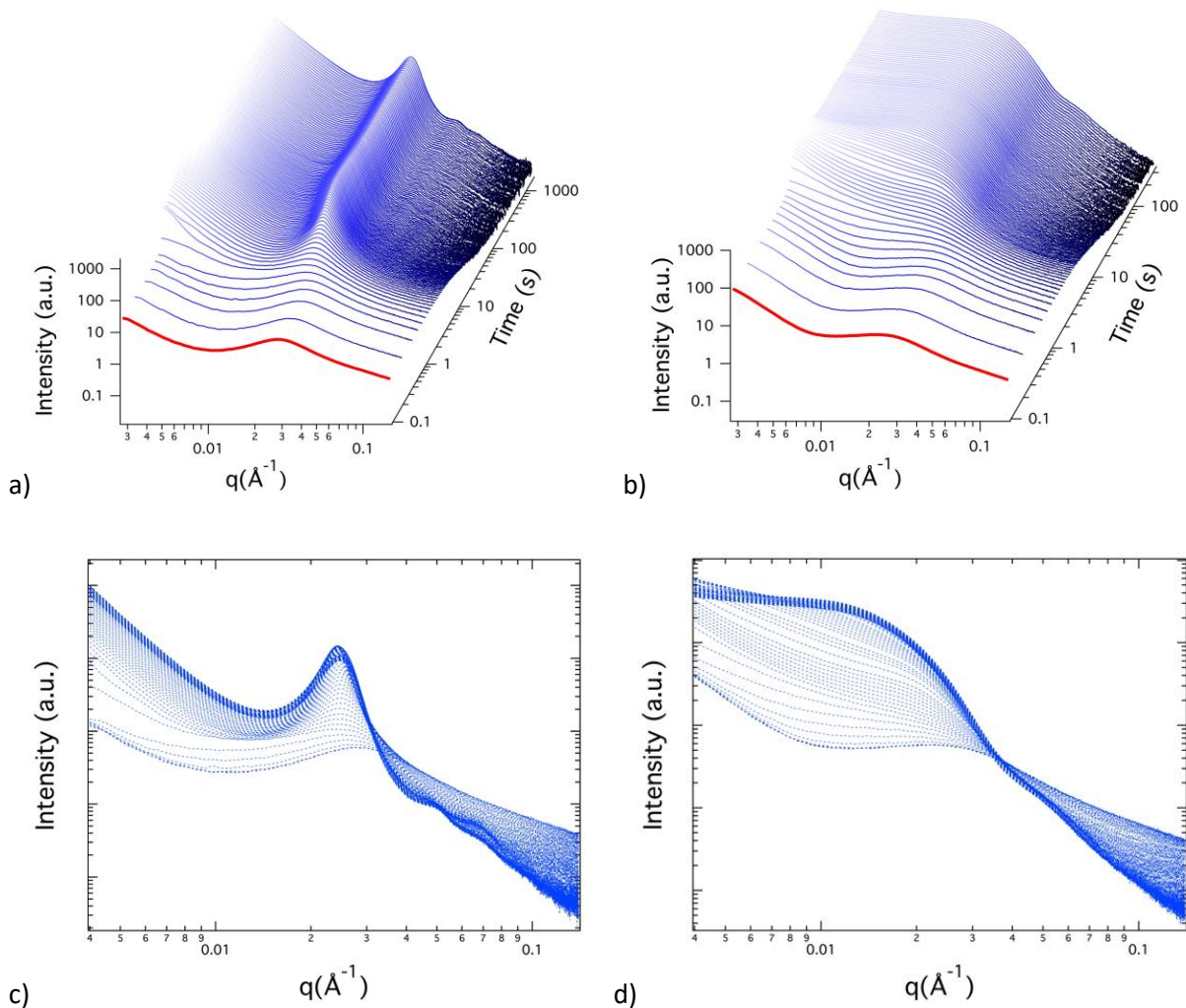


Figure 6. Time-resolved SAXS patterns collected on $30T_{AP}PI_{0.5}$ (a) and $30T_{NMRP}PI_{0.5}$ (b) formulations under UV versus exposure time. The red SAXS patterns correspond to the formulations before UV exposure. (c) and (d) plots present all the scattering patterns from Figures (a) and (b) respectively to highlight the iso-scattering point.

To monitor and better describe the out of equilibrium self-assembly process, in situ time-resolved SAXS experiments were performed during photopolymerization. Figure 6a and Figure 6b present typical series of spectra collected on $30T_{AP}PI_{0.5}$ and $30T_{NMRP}PI_{0.5}$ formulations. The scattering pattern evolutions are different for both formulations, despite rather comparable initial spectra. During the first seconds, the scattering patterns present a broad peak indicating a mixed state of triblock copolymers ABA in monomers and possibly oligomers B. Also, the final spectra are comparable to the ones observed on the regular films (Figure 5). Similar behaviors are observed for all formulations (Figure S11).

The plot of the scattering patterns collected on sample 30T_{NMRP}PI_{0.5} during photopolymerization reveals an isoscattering (or isobestic scattering) point, independent of polymerization time, at 0.0365 Å⁻¹ (Figure 6d). Isoscattering point are commonly associated to microphase separation processes, where the scattering patterns versus q are linear combinations of two q -functions corresponding to initial and final states of the scattering object.^[58-60] In the present system, this feature is interpreted as the signature of a transition from BCPs in solution to the kinetically trapped BCP aggregates. An isoscattering point is observed for all 30T_{NMRP} formulations as shown on Figure S12. On the other hand, no evident isoscattering point is observed for sample 30T_{AP}PI_{0.5} (Figure 6c). However, a limited crossing area is distinguishable in q -range 0.03 to 0.04 Å⁻¹; also observed for the other 30T_{AP} formulations (Figure S12). This deviation from an isoscattering point do not exclude microphase separation processes. It can be explained by the growing structure factor with polymerization time. Consequently, a basic linear combination of two q -functions is not sufficient to fully describe the scattering patterns evolution.

To further analyze the SAXS data, low- q power law exponent, peak intensity and peak full width at half maximum (*FWHM*, for T_{AP} series only) were extracted as function of polymerization time. Regarding T_{NMRP} series, peak intensities were extracted from the maximum of the $I.q^2$ curves. Those features, presented in Figure 7 and Figure 8, allow to monitor the macrophase and microphase separations. Indeed, a low- q power law with a -4 exponent, is the signature of a macrophase segregation with a sharp interface, i.e., Porod's law. On the other hand, structural peak intensity and *FWHM* evolution inform on the microphase separation process.^[61]

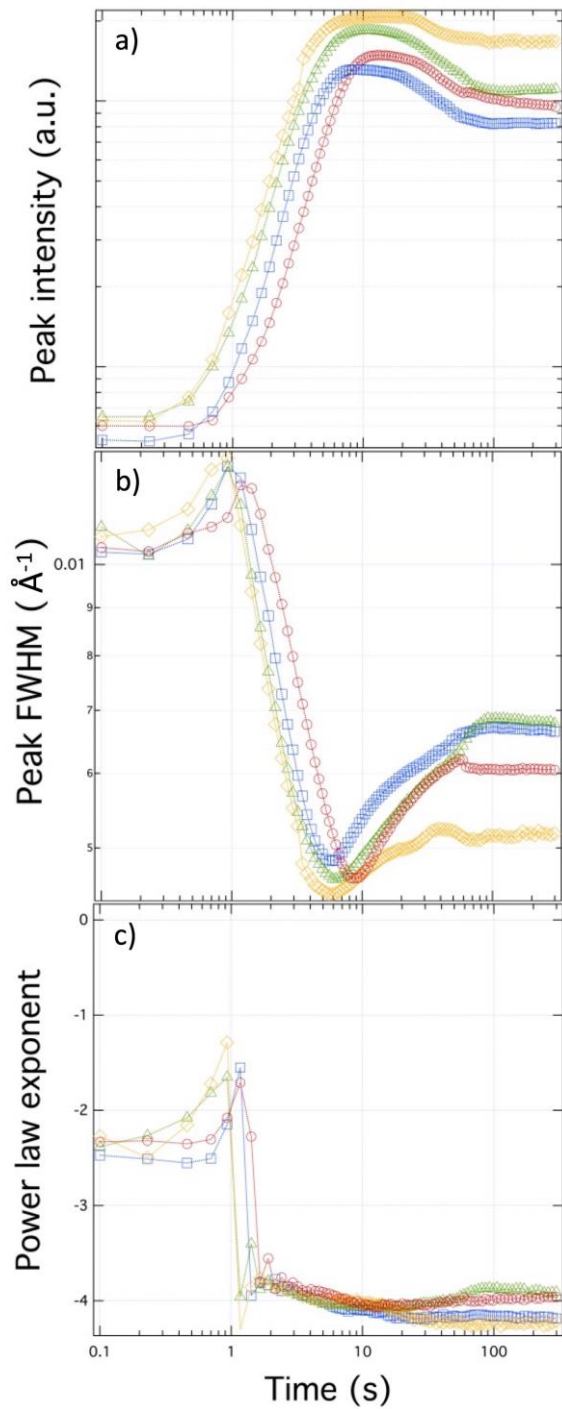


Figure 7. Analysis of time-resolved SAXS experiments measured on formulations 30T_{AP}PI_{0.5} (open red circle) 30T_{AP}PI₁ (open blue square), 30T_{AP}PI₂ (open green triangle) and 30T_{AP}PI₄ (open orange diamond): (a) SAXS peak intensity (log scale), (b) peak *FWHM* (log scale) and (c) low-*q* power law exponent versus UV exposure time (300 s).

Regarding T_{AP} series (Figure 7c), the low- q power law starts with an exponent of -2.5, followed by a slight increase associated with a shift of the initial broad peak towards smaller q (Figure 6c). More interestingly, between 1 and 2 seconds, a sharp transition towards a -4 exponent occurs for all PI concentrations, indicating the sharp rising of the macrophase separation. In parallel, peak intensity and $FWHM$ follow a transition, between 1 and 10 seconds (cf. Figure 7a and b). Indeed, the intensity increases sharply with time and $FWHM$ gets narrower, indicating the occurrence of the microphase separation. The same general behaviors are observed for all PI contents. However, the transitions are systematically shifting slightly towards shorter times when increasing PI content. That indicates that self-assembly process, at both micro- and macro-scales, are accelerated with an increasing PI content.

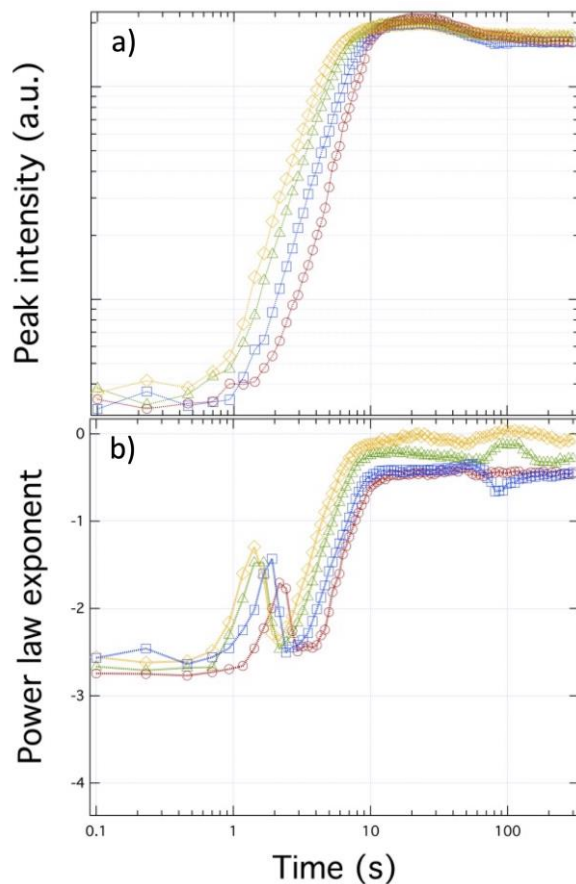


Figure 8. Analysis of time-resolved SAXS experiments measured on formulations $30T_{NMRP}PI_{0.5}$ (open red circle) $30T_{NMRP}PI_1$ (open blue square), $30T_{NMRP}PI_2$ (open green triangle) and $30T_{NMRP}PI_4$ (open orange diamond). (a) SAXS peak intensity (log scale) and (b) low- q power law exponent versus UV exposure time (300 s).

Regarding T_{NMRP} series kinetic analysis (Figure 8b), similarly to the T_{AP} series, the low- q power law exponent is starting around -2.5, followed after 1 second by a slight increase also associated with a shift of the initial broad peak toward small q (Figure 6d). Then a systematic and time limited decrease is detected.

Typically, between 2 and 4 seconds, which might correspond to the macrophase separation activation. Finally, a significant exponent increase towards 0 is observed and attributed to the rising of the microphase aggregation scattering (i.e., spherical form factor), which overtakes the ill-defined macrophase separation scattering. That growing microphase aggregation can be monitored via the maximum peak intensity, presented on Figure 8a. A broad transition is observed, between 1 and 10 seconds. Identical behaviors are observed for all formulation, with slightly faster kinetics when PI content increases.

For both formulation series, the quasi-final morphologies are achieved after 10 seconds. The weak final evolution (after 10 seconds) can be attributed to the remaining monomers diffusion within the frozen morphology. Since, monomer conversions monitored by time-resolved FTIR indicates that polymerization is still on-going well after 10 seconds (Figure 1).

To summarize, kinetic SAXS experiment analysis on $30T_{AP}$ series indicates that full macrophase separation, between BCP and homopolymer rich domains, is brief and occurs ahead of the BCP microphase separation. Indeed, in BCP rich domains the microphase segregation is more progressive. On the other hand, on T_{NMRP} series a limited macrophase separation associated with a diffuse microphase segregation are observed. Actually, the extension of the reactive T_{NMRP} BCP by $PnBA$ chains during polymerization allows a better stabilization of the copolymers within the nBA monomer and $PnBA$ homopolymers domains, thus limiting the macrophase separation.

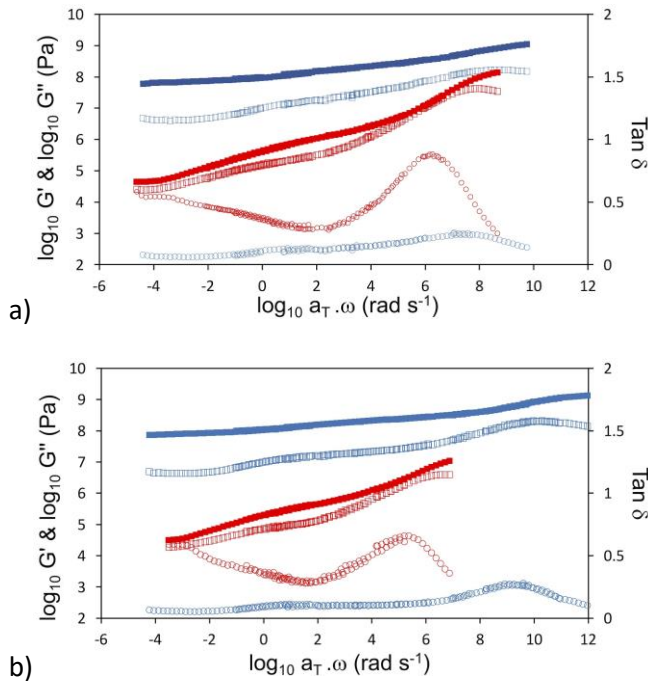


Figure 9. (a) Spectromechanical master curves for the T_{NMRP} BCP (blue markers) and $30T_{NMRP}PI_{0.5}$ (red markers). (b) Spectromechanical master curves versus frequency for the T_{AP} BCP (blue markers) and $30T_{AP}PI_{0.5}$ (red markers). Solid

square corresponds to G' , open square to G'' and open circle to $Tan\delta$. The master curves reference temperature is $T_{ref} = 20\text{ }^{\circ}\text{C}$.

Spectromechanical analysis. Figure 9 presents the spectromechanical master curves measured on the BCP and formulated samples. The time-temperature equivalence is applied to build up the master curves by successive horizontal translations.^[62, 63] The translation coefficients, aT , are adjusted using a *WLF* law,^[64] with $20\text{ }^{\circ}\text{C}$ as reference temperature, T_{ref} . The resulting coefficients $C1$ and $C2$ are presented in ESI, Table S4 and Table S5.

Both BCPs present rather similar rheological signatures (Figure 9a and b), with G' higher than G'' over all frequency range, consistent with their block structure. At high frequency, *PnBA* and *PMMA* blocks are both in glassy state displaying high elastic modulus, i.e., $G' \approx 10^9\text{ Pa}$. On the other hand, at low frequency, a plateau domain corresponding to the signature of a solid-like behavior is observed. The occurrence of this plateau can be explained by the entangled *PnBA* block which are constrained by the microphase segregation and consequently cannot relax. This rheological behavior is in agreement with the observations reported previously by Jullian *et al.* on similar triblock copolymers.^[20]

Figure 9a allows a comparison between T_{NMRP} BCP and sample $30T_{NMRP}PI_{0.5}$. G' and G'' moduli, measured on sample $30T_{NMRP}PI_{0.5}$ are significantly lower than those of T_{NMRP} BCP. This is explained by the additional 70 wt-% of *PnBA* soft homopolymer. Although, the glassy domain is not well marked for $30T_{NMRP}PI_{0.5}$ formulation, the transition between the glassy domain and the plateau modulus is located in a frequency range comparable to the T_{NMRP} BCP sample. This specific transition corresponds to the relaxation of the soft *PnBA* block. Interestingly, the characteristic *PnBA* homopolymer terminal region,^[56] does not appear in the formulated sample, despite a *PnBA* majority phase. This is attributed to the phase segregation which persists in the formulated sample and induces the observed solid-like behavior. Similar behaviors are observed for all the other $30T_{NMRP}$ formulations (Figure S14). The comparison between T_{AP} BCP and sample $30T_{AP}PI_{0.5}$ (Figure 9b) leads to identical conclusions, which can also be extended to the $30T_{AP}$ series (Figure S15). Overall and notably, all formulated samples exhibit a solid-like behavior despite a total *PnBA* content of about 85 wt-%.

Although, the global rheological signatures of the $30T_{AP}$ and $30T_{NMRP}$ formulated samples are rather similar, their elastic modulus, G' , measured at low frequencies diverge. Indeed, G' values measured on $30T_{NMRP}$ series increase marginally with PI content (Table S4). Whereas G' value measured on $30T_{NMRP}$ series reveal an evident increase (Table S5). This evolution is not consistent with *PnBA* homopolymer molar mass decreases when PI content increases, as shown by SEC on Figure 2a. Thus, one can expect that the residual

*n*BA monomer, which decreases when PI content increases (Table 2), induces a swelling effect. Consequently, it lowers the elastic modulus. In order to avoid residual monomer impact, G' values measured on the formulated samples containing the highest amount of PI (4 wt-%) can be compared (Table S4 and Table S5). Sample 30T_{AP}PI₄ displays an elastic modulus, at low frequency, a decade higher than 30T_{NMRP}PI₄ sample. This significant modulus improvement might be correlated to the hierarchical morphology differences. Essentially, sample 30T_{NMRP}PI₄ sample exhibit diffuse macrophase and microphase separations (Figure S9). Whereas sample 30T_{AP}PI₄ exhibits a percolating network of densely packed nano-structured BCPs (Figure S10) reinforcing mechanical properties.

Conclusions

The photopolymerization process developed in this paper allows a control on concomitant macrophase and microphase separations to produce an acrylate based hierarchical thermoplastic elastomer. Firstly, the reactive and inert characters of both triblock copolymers during photopolymerization was demonstrated and associated to their respective polymerization route: NMRP versus AP respectively. The structural analysis performed on the photopolymerized films reveals hierarchical morphologies that can be described as networks of high T_g PMMA nodules surrounding macro-domains of low T_g *Pn*BA; with *Pn*BA the majority phase, i.e., 85 wt-%. The time-resolved analysis points out the strong interaction between *n*BA polymerization kinetics and BCP self-assembly. More specifically, it is shown that the macrophase separation, controlled by the block copolymer reactivity, is triggered by polymerization in the very first seconds. Also, the properties of final solid materials are controlled by the hierarchical morphology. The optical transparency is well correlated with the characteristic of macrophase separation and surprisingly the materials remain easily handleable at room temperature despite a composition of 85 wt-% of *Pn*BA. Spectromechanical analysis confirms the later observation since the terminal region, characteristic of the *Pn*BA homopolymer, does not appear on formulated PIMS/PIPS samples. This is associated to the persistence of the phase segregations inducing a solid-like behavior. In addition, the non-reactive BCP hierarchical structure, i.e., percolating network of densely packed nano-structured BCPs, leads to superior mechanical properties. Finally, and interestingly, the materials produced in this work can be easily processed by close molding and easily recycled since no solvent and no crosslinker are used.

Supporting Information

Supporting Information is available from the Wiley Online Library or from the author.

Acknowledgements

The authors thank the project ISOCEL (Innovative Solar Cells) coordinated by the technological transfer platform CANOE. This project was selected by ADEME (French Agency for Ecological Transition) and funded by the Conseil Régional de Nouvelle Aquitaine (CRNA) and the State of France (programme Investissements d'Avenir). We are grateful to the Arkema research team for their technical support and fruitful discussions during the project. Arkema and Kuraray companies are thanked for providing the triblock copolymers used in the study. F. Ehrenfeld and A. Laffore are thanked for their help to build up the time-resolved FTIR setup. We acknowledge SOLEIL for provision of synchrotron radiation facilities and we would like to thank T. Bizien and J. Perez for assistance in using SAXS beamline SWING. We acknowledge also ALBA synchrotron for additional SAXS experiments, performed at BL11-NCD beamline with support of M. Malfois and ALBA staff.

Conflict of Interest

The authors declare no conflict of interest.

Data Availability Statement

The data that support the findings of this study are available from the corresponding author upon reasonable request.

References

- [1] W. Wang, W. Lu, A. Goodwin, H. Wang, P. Yin, N.-G. Kang, K. Hong, J. W. Mays, *Progress in Polymer Science* **2019**, *95*, 1.
- [2] USA. US3265765A (1966), Shell USA Inc, invs.: G. Holden, R. Milkovich;
- [3] F. S. Bates, K. A. Koppi, M. Tirrell, K. Almdal, K. Mortensen, *Macromolecules* **1994**, *27*, 5934.
- [4] F. S. Bates, J. H. Rosedale, G. H. Fredrickson, *The Journal of Chemical Physics* **1990**, *92*, 6255.

- [5] B. Dufour, K. Koynov, T. Pakula, K. Matyjaszewski, *Macromolecular Chemistry and Physics* **2008**, *209*, 1686.
- [6] L. Lalande, C. J. G. Plummer, J.-A. E. Månson, P. Gérard, *Polymer* **2006**, *47*, 2389.
- [7] P. Gerard, L. Couvreur, S. Magnet, J. Ness, S. Schmidt, "Controlled Architecture Polymers at Arkema: Synthesis, Morphology and Properties of All-Acrylic Block Copolymers", in *Controlled/Living Radical Polymerization: Progress in RAFT, DT, NMP & OMRP*, 2009, p. 361.
- [8] L. Leibler, *Macromolecules* **1980**, *13*, 1602.
- [9] F. S. Bates, *Science* **1991**, *251*, 898.
- [10] G. H. Fredrickson, F. S. Bates, *Annu Rev Mater Sci* **1996**, *26*, 501.
- [11] A. V. Ruzette, S. Tencé-Girault, L. Leibler, F. Chauvin, D. Bertin, O. Guerret, P. Gérard, *Macromolecules* **2006**, *39*, 5804.
- [12] J. M. Widin, A. K. Schmitt, A. L. Schmitt, K. Im, M. K. Mahanthappa, *Journal of the American Chemical Society* **2012**, *134*, 3834.
- [13] A. K. Schmitt, M. K. Mahanthappa, *Macromolecules* **2014**, *47*, 4346.
- [14] M. W. Matsen, R. B. Thompson, *J Chem Phys* **1999**, *111*, 7139.
- [15] M. W. Matsen, *Eur. Phys. J. E* **2013**, *36*.
- [16] T. A. Mykhaylyk, O. O. Mykhaylyk, S. Collins, I. W. Hamley, *Macromolecules* **2004**, *37*, 3369.
- [17] V. Abetz, P. F. W. Simon, "Phase behaviour and morphologies of block copolymers", in *Advances in Polymer Science*, 2005, p. 189/125.
- [18] R. L. Roberge, N. P. Patel, S. A. White, W. Thongruang, S. D. Smith, R. J. Spontak, *Macromolecules* **2002**, *35*, 2268.
- [19] F. X. Gibert, G. Marin, C. Derail, A. Allal, J. Lechat, *J Adhes* **2003**, *79*, 825.
- [20] N. Jullian, L. Rubatat, P. Gerard, J. Peyrelasse, C. Derail, *J Rheol* **2011**, *55*, 379.

- [21] W. Shi, A. L. Hamilton, K. T. Delaney, G. H. Fredrickson, E. J. Kramer, C. Ntaras, A. Avgeropoulos, N. A. Lynd, Q. Demassieux, C. Creton, *Macromolecules* **2015**, *48*, 5378.
- [22] J. Lequieu, A. J. D. Magenau, *Polymer Chemistry* **2021**, *12*, 12.
- [23] T. Oh, S. Cho, C. Yoo, W. Yeo, J. Oh, M. Seo, *Progress in Polymer Science* **2023**, *145*.
- [24] K. Lee, N. Corrigan, C. Boyer, *Angew Chem Int Ed Engl* **2023**, *62*, e202307329.
- [25] L. D. McIntosh, M. W. Schulze, M. T. Irwin, M. A. Hillmyer, T. P. Lodge, *Macromolecules* **2015**, *48*, 1418.
- [26] N. Kimura, K. Kawazoe, H. Nakanishi, T. Norisuye, Q. Tran-Cong-Miyata, *Soft Matter* **2013**, *9*, 8428.
- [27] Q. Tran-Cong-Miyata, T. Kinohira, D. T. Van-Pham, A. Hirose, T. Norisuye, H. Nakanishi, *Curr. Opin. Solid State Mater. Sci.* **2011**, *15*, 254.
- [28] T. Shukutani, T. Myojo, H. Nakanishi, T. Norisuye, Q. Tran-Cong-Miyata, *Macromolecules* **2014**, *47*, 4380.
- [29] Q. Tran-Cong-Miyata, H. Nakanishi, *Polym. Int.* **2017**, *66*, 213.
- [30] Y. Furubayashi, R. Kawakubo, H. Nakanishi, T. Norisuye, Q. Tran-Cong-Miyata, *Chaos* **2015**, *25*.
- [31] M. Fischer, G. P. Hellmann, *Macromolecules* **1996**, *29*, 2498.
- [32] F. J. Enríquez-Medrano, F. Soriano-Corral, P. Acuña-Vázquez, E. N. Cabrera-Álvarez, H. Saade-Caballero, A. Castañeda-Facio, L. V. López, R. D. de León-Gómez, *Journal of the Mexican Chemical Society* **2014**, *58*, 194.
- [33] M. W. Schulze, C. Sinturel, M. A. Hillmyer, *ACS Macro Lett.* **2015**, *4*, 1027.
- [34] J. Oh, M. Seo, *ACS Macro Letters* **2015**, *4*, 1244.
- [35] B. Yan, J. He, Y. Fang, X. Du, Q. Zhang, S. Wang, C. Pan, Y. Wang, *European Polymer Journal* **2009**, *45*, 1936.
- [36] Y. Z. You, C. Y. Hong, R. K. Bai, C. Y. Pan, J. Wang, *Macromolecular Chemistry and Physics* **2002**, *203*, 477.

- [37] T. G. McKenzie, Q. Fu, E. H. H. Wong, D. E. Dunstan, G. G. Qiao, *Macromolecules* **2015**, *48*, 3864.
- [38] A. Malafrente, I. W. Hamley, D. Hermida-Merino, F. Auriemma, C. De Rosa, *Polymer* **2021**, 237.
- [39] F. Meng, S. Zheng, W. Zhang, H. Li, Q. Liang, *Macromolecules* **2005**, *39*, 711.
- [40] F. Meng, S. Zheng, H. Li, Q. Liang, T. Liu, *Macromolecules* **2006**, *39*, 5072.
- [41] Z. Xu, S. Zheng, *Macromolecules* **2007**, *40*, 2548.
- [42] R. Yu, S. Zheng, *Macromolecules* **2011**, *44*, 8546.
- [43] J. M. Dean, P. M. Lipic, R. B. Grubbs, R. F. Cook, F. S. Bates, *Journal of Polymer Science Part B: Polymer Physics* **2001**, *39*, 2996.
- [44] L. Chen, W. A. Phillip, E. L. Cussler, M. A. Hillmyer, *J Am Chem Soc* **2007**, *129*, 13786.
- [45] M. A. Amendt, L. Chen, M. A. Hillmyer, *Macromolecules* **2010**, *43*, 3924.
- [46] J. Park, S. A. Saba, M. A. Hillmyer, D.-C. Kang, M. Seo, *Polymer* **2017**, *126*, 338.
- [47] M. Seo, S. Kim, J. Oh, S. J. Kim, M. A. Hillmyer, *J Am Chem Soc* **2015**, *137*, 600.
- [48] B. Deore, K. L. Sampson, T. Lacelle, N. Kredentser, J. Lefebvre, L. S. Young, J. Hyland, R. E. Amaya, J. Tanha, P. R. L. Malenfant, H. W. de Haan, C. Paquet, *Nat Commun* **2021**, *12*, 55.
- [49] Z. Dong, H. Cui, H. Zhang, F. Wang, X. Zhan, F. Mayer, B. Nestler, M. Wegener, P. A. Levkin, *Nat Commun* **2021**, *12*, 247.
- [50] V. A. Bobrin, K. Lee, J. Zhang, N. Corrigan, C. Boyer, *Adv Mater* **2021**, e2107643.
- [51] V. A. Bobrin, Y. Yao, X. Shi, Y. Xiu, J. Zhang, N. Corrigan, C. Boyer, *Nat Commun* **2022**, *13*, 3577.
- [52] X. Shi, Y. Yao, J. Zhang, N. Corrigan, C. Boyer, *Small* **2023**, e2305268.
- [53] C. Dire, J. Belleney, J. Nicolas, D. Bertin, S. Magnet, B. Charleux, *Journal of Polymer Science Part A: Polymer Chemistry* **2008**, *46*, 6333.
- [54] N. Cherifi, A. Khoukh, A. Benaboura, L. Billon, *Polymer Chemistry* **2016**, *7*, 5249.

- [55] D. M. Haddleton, D. R. Maloney, K. G. Suddaby Adam Clarke, S. N. Richards, *Polymer* **1997**, *38*, 6207.
- [56] N. Jullian, F. Leonardi, B. Grassl, J. Peyrelasse, C. Derail, *Applied Rheology* **2010**, *20*.
- [57] D. J. Kinning, E. L. Thomas, *Macromolecules* **1984**, *17*, 1712.
- [58] N. Baccile, A. S. Cuvier, S. Prevost, C. V. Stevens, E. Delbeke, J. Berton, W. Soetaert, I. N. A. Van Bogaert, S. Roelants, *Langmuir* **2016**, *32*, 10881.
- [59] M. Chalal, F. Ehrburger-Dolle, I. Morfin, F. Bley, M.-R. Aguilar de Armas, M.-L. López Donaire, J. San Roman, N. Bölgen, E. Pişkin, O. Ziane, R. Casalegno, *Macromolecules* **2010**, *43*, 2009.
- [60] T. Nicolai, M. Pouzot, D. Durand, M. Weijers, R. W. Visschers, *Europhysics Letters (EPL)* **2006**, *73*, 299.
- [61] A.-V. r. G. Ruzette, P. P. Soo, D. R. Sadoway, A. M. Mayes, *Journal of The Electrochemical Society* **2001**, *148*, A537.
- [62] A. K. Doolittle, *Journal of Applied Physics* **1951**, *22*, 1471.
- [63] J. D. Ferry, "*Viscoelastic Properties of Polymers*", John Wiley & Sons, 1980.
- [64] M. L. Williams, R. F. Landel, J. D. Ferry, *Journal of the American Chemical Society* **2002**, *77*, 3701.
-